

NUMERICAL ANALYSIS FOR TURBULENT FLOW STRUCTURE IN TWO RECTANGULAR CHANNELS CONNECTED BY A NARROW GAP

Naoto KATO

Utsunomiya University
7-1-2 Yoto, Utsunomiya, Tochigi,
Japan,
+81-28-689-6032,
note@cc.utsunomiya-u.ac.jp

Takaya SAITO

Utsunomiya University
7-1-2 Yoto, Utsunomiya, Tochigi,
Japan,
+81-28-689-6032,
mt146625@cc.utsunomiya-u.ac.jp

Hitoshi SUGIYAMA

Utsunomiya University
7-1-2 Yoto, Utsunomiya, Tochigi,
Japan,
+81-28-689-6031,
sugiyama@cc.utsunomiya-u.ac.jp

Atsuhiko TERADA

Japan Atomic Energy Agency
4002 Narita-cho, Oarai,
Higashi-Ibaraki, Ibaraki, Japan,
+81-29-267-1919 ext.3841
terada.atsuhiko@jaea.go.jp

Yu KAMIJI

Japan Atomic Energy Agency
4002 Narita-cho, Oarai,
Higashi-Ibaraki, Ibaraki, Japan,
+81-29-267-1919 ext.3844
kamiji.yu@jaea.go.jp

Ryutaro HINO

Japan Atomic Energy Agency
4002 Narita-cho, Oarai,
Higashi-Ibaraki, Ibaraki, Japan,
+81-29-267-1919 ext.7154
terada.atsuhiko@jaea.go.jp

Keywords: Turbulent Flow, Numerical Simulation, Pipe Flow, Algebraic Reynolds Stress Model, Hydrogen, Safety Measures.

ABSTRACT

A large scale pulsation that oscillates in a narrow gap that connects two rectangular channels is observed. The phenomenon is similar to the mixing of cooling fluid in rod bundles of power plants from one sub-channel to another through the gaps between the rods.

The fluid mixing in rod bundles has been studied from 1960s to the present time to predict the temperature distributions of the rods and the cooling fluid in a nuclear reactor that were used when a power plant was designed for its safety assessment. The nature of the fluid mixing has been accounted for by turbulence and secondary flows, which also occur in the turbulent flow field. Recently, hot wire measurement revealed that the fluid mixing was periodic and coupled with Reynolds number and the gap geometry. In addition, the visualization of the flow in a rectangular channel containing a cylindrical rod showed the existence of a vortex in the narrow gap between the rod and the channel and it also accounted for the fluid mixing. The amplitude of the visualized vortex seems to become larger as it flows downstream, however the cause of the amplitude increase has not discussed yet.

In this study, a numerical analysis has been performed in a composed channel consisting of two rectangular channels which are connected by a narrow gap near a wall. An algebraic Reynolds stress model is used to predict Reynolds

stresses in the channel precisely. Calculated results for axial mean velocity, streamwise and gap-parallel turbulence intensities are compared to the experimental data to validate the proposed numerical model. The proposed model can predict characteristic isocontours of axial mean velocity, streamwise turbulence intensity and gap-parallel turbulent shear stress, although quantitative differences are observed in several predictions from experimental data. Calculated planar turbulent shear stress and secondary flows near the gap are shown to compare with the result by large eddy simulation. In the gap region, velocity vectors show the large scale pulsation that is also observed in the experiment. Streamwise variations of axial mean velocity and axial velocity fluctuation, turbulence intensity and turbulent shear stresses of the gap center are discussed as an indication of the leading point of the large scale pulsation.

1. INTRODUCTION

The flow behavior in a channel has been of major interest for researchers. Lots of experimental and analytical reports have been presented and they have been applied to the designs and safety assessments of the nuclear power plants. Meyer (2010) reviewed the flow mechanism in the channel or in the rod bundles of the experimental investigations and code applications. In the case of the flow through the rod bundles, inter-channel mixing rate is observed that flows

from one sub-channel to another. Guellouz et al. (2000) observed the same mixing rate in the small gap in the rectangular channel containing a cylindrical rod. It seems that the gap connects two large channels and that the mixing flow is inter-channel mixing. It is called large scale pulsation and its periodicity is confirmed. Biemüller et al. (1996) also found the large scale pulsation in the gap connecting two rectangular channels in the wind tunnel experiment and the LES analysis although the cross-section is assumed to be infinite in the horizontal direction for the simulation. Near the corners of the rectangular channel without cylinders, the contour lines of the averaged axial (streamwise) velocity were bulged and Meyer introduced the explanation by Prandtl that the reason for the bulged lines was the fact that the turbulent mixing parallel to walls was stronger than the perpendicular one to them. The mean velocity of the flow near the gap connecting the two rectangular channels was larger than that near the other corners. The inter-channel flow through the gap was suggested to stretch the line towards the gap. Sugiyama et al. (2014) calculated the flow of a rectangular channel containing a cylindrical rod and showed the relationship between the horizontal instantaneous velocity profile and the averaged one.

In this paper the result of numerical prediction is presented for the turbulent flow in two rectangular channels with a gap connecting one to another, as reported by Biemüller, in order to estimate the validity of an algebraic Reynolds stress model. In addition, the effect on the flow behavior of the turbulent energy of the inlet flow is discussed. The vorticity field is visualized in the gap plane and quasi-periodicity is confirmed.

NOMENCLATURE

D	hydraulic diameter
k	turbulent energy
P	mean pressure
p	fluctuating pressure
P_k	production term of turbulent energy
$u_i u_j$	Reynolds stresses
U_b	bulk velocity
U_i	velocity in the direction of the X_i -axis
U_τ	friction velocity
X_i	location of the X_i -axis
t	time
δ_{ij}	Kronecker delta
ε	turbulent dissipation
ν	kinematic viscosity

2. ANALYSIS

2.1 Numerical Object and Definition of the Coordinate System

Figure 1 shows the cross-section of the two rectangular channels connected by the small gap that is selected as numerical objects and the coordinate system in this study. Biemüller et al. measured the turbulent flow in these channels by using a hot wire anemometer. The experimental sub-channels had a width of 145.5 mm, a height of 180 mm and a length of 7 m. These sub-channels were connected by the gap that had a width of 40.6 mm and a height of 10.2 mm. The measurements were performed at 6.97 m from the inlet.

The Reynolds number was 2.0×10^5 based on the hydraulic diameter, $D = 166.3$ mm, and bulk velocity, U_b . The coordinate systems used in the calculation are also defined in this figure. In the rectangular channel, the axial flow direction is represented by the X_1 -axis and the secondary flow directions are denoted by the X_2 - and X_3 -axes, which represent the horizontal and vertical directions, respectively.

2.2 Governing Transport Equations

The transport equation of momentum is expressed in the following form through the ensemble-averaged operation and is indispensable in solving the Reynolds stresses that appear in the transport equation in order to completely obtain the velocity fields

$$\frac{D\bar{U}_i}{Dt} = -\frac{1}{\rho} \frac{\partial \bar{P}}{\partial X_i} + \frac{\partial}{\partial X_j} \left(\nu \frac{\partial \bar{U}_i}{\partial X_j} - \overline{u_i u_j} \right). \quad (1)$$

In this calculation, the transport equation of Reynolds stresses has been adopted to predict the anisotropic turbulence accurately. The transport equation of Reynolds stresses is expressed exactly as follows:

$$\begin{aligned} \frac{D\overline{u_i u_j}}{Dt} = & - \left(\overline{u_i u_k} \frac{\partial U_j}{\partial X_k} + \overline{u_j u_k} \frac{\partial U_i}{\partial X_k} \right) + \frac{p}{\rho} \left(\frac{\partial u_i}{\partial X_j} + \frac{\partial u_j}{\partial X_i} \right) \\ & - \frac{\partial}{\partial X_k} \left\{ \left(\overline{u_i u_j u_k} - \nu \frac{\partial \overline{u_i u_j}}{\partial X_k} + \frac{p}{\rho} (\delta_{jk} u_i + \delta_{ik} u_j) \right) \right\} \\ & - 2\nu \frac{\partial u_i}{\partial X_k} \frac{\partial u_j}{\partial X_k}. \end{aligned} \quad (2)$$

It is impossible to solve Equation (2) directly and numerically. Therefore, it is necessary to rewrite several terms of the Reynolds stress equation by introducing the concept of the turbulent model. Moreover, in numerical analysis, the convection term on the left-hand side and the diffusion term on the right-hand side are obstacles in obtaining a numerical solution because these terms are required to carry out iterative calculations to obtain the stable results. These terms are modeled by adopting the approximation by Rodi (1976)

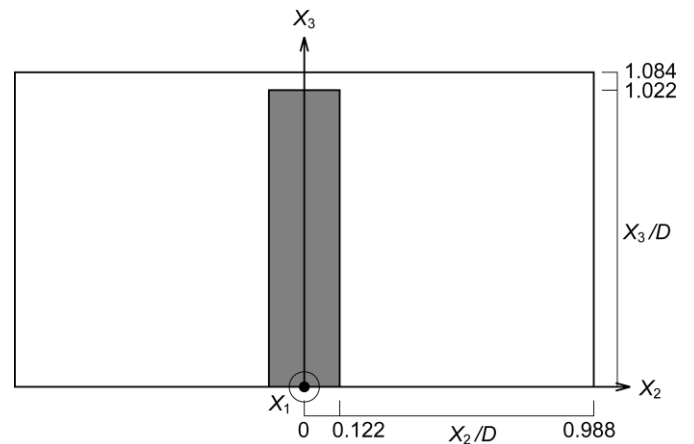


Fig. 1 Cross-section of the two rectangular channels connected by the small gap and the coordinate system
Copyright © 2014-2015 by JSME

Table 1 Modeling of the pressure-strain correlation term

$\pi_{i,j,1} + \pi_{j,i,1}$	$-C_1 \frac{\varepsilon}{k} \left(\overline{u_i u_j} - \frac{2}{3} k \delta_{ij} \right)$
$\pi_{i,j,2} + \pi_{j,i,2}$	$-\frac{C_2 + 8}{11} \left(P_{ij} - \frac{2}{3} P_k \delta_{ij} \right) + \zeta k \left(\frac{\partial U_i}{\partial x_j} + \frac{\partial U_j}{\partial x_i} \right) - \frac{8C_2 + 2}{11} \left(D_{ij} - \frac{2}{3} P_k \delta_{ij} \right)$
$[\pi_{ij} + \pi_{ji}]_w$	$C_1 = C_1^* + C_1' f \left(\frac{L}{X_w} \right), \quad C_2 = C_2^* + C_2' f \left(\frac{L}{X_w} \right), \quad \zeta = \zeta^* + f \left(\frac{L}{X_w} \right)$
	$P_{ij} = -\overline{u_i u_k} \frac{\partial U_i}{\partial x_k} - \overline{u_j u_k} \frac{\partial U_j}{\partial x_k}, \quad D_{ij} = -\overline{u_i u_k} \frac{\partial U_k}{\partial x_j} - \overline{u_j u_k} \frac{\partial U_k}{\partial x_i}$ $P_k = -\overline{u_k u_l} \frac{\partial U_k}{\partial x_l}, \quad f \left(\frac{L}{X_w} \right) = \frac{C_\mu^{3/4}}{\kappa} k^{3/2} \frac{1}{\varepsilon X_w}$

in this study. As a result of this approximation, these two terms are transformed into an algebraic form. Therefore, the convection and diffusion terms in Equation (2) were modeled as follows:

$$\frac{D\overline{u_i u_j}}{Dt} - \text{Diff}_{ij} = \frac{\overline{u_i u_j}}{2k} (P_k - \varepsilon) \quad (3)$$

where Diff_{ij} corresponds to the third term on the right-hand side of Equation (2) and P_k represents the production term of the turbulent energy equation.

A particularly problematic task here is the modeling of the pressure-strain correlation equation term, which is also defined as the redistribution term and is shown as the second term on the righthand side of Equation (2). The pressure-strain term is composed of three parts, which are the interaction of the fluctuating velocities ($\pi_{i,j,1} + \pi_{j,i,1}$), the interaction of the mean strain with the fluctuating velocities ($\pi_{i,j,2} + \pi_{j,i,2}$), and the wall proximity effects ($\pi_{i,j,w} + \pi_{j,i,w}$). In the present calculation, we have adopted Rotta's linear return to isotropy mode for the ($\pi_{i,j,1} + \pi_{j,i,1}$) term, as shown in Table 1.

For $\pi_{i,j,2}$, the correlation is approximated as

$$\pi_{i,j,2} = \left(\frac{\partial U_l}{\partial X_m} \right) a_{ij}^{mi} \quad (4)$$

and a_{ij}^{mi} is the fourth-order tensor, which should satisfy the following kinematic constraints:

$$a_{ij}^{mi} = a_{ij}^{im} = a_{ji}^{im}, \quad (5)$$

$$a_{ij}^{mi} \frac{\partial U_l}{\partial X_m} = 0, \quad (6)$$

$$a_{ij}^{mi} = 2\overline{u_m u_i}. \quad (7)$$

The above constraints arise from the symmetry condition, the mass conservation law, and Green's theorem, respectively. Although the kinematic constraint of Equation (6) is different

from that reported by Launder et al. (1975), we adopted Equation (6) because $\pi_{i,j,2}$ is defined as the production between the fourth-order tensor and the mean strain, as shown in Equation (4). Gessner and Eppich (1981) have also reported these constraints and described them in detail. In terms of the modeling of ($\pi_{i,j,2} + \pi_{j,i,2}$), the modeling process is described in detail in a previous report by Sugiyama and Hitomi (2005). In addition, Sugiyama et al. (2006) have confirmed the validity of the presented model by the calculation carried out for a turbulent flow in a meandering open-channel flow. In this case, the boundary condition along the free surface and the turbulent model are important factors to precisely predict the open-channel flow because anisotropic turbulence is produced near the free surface. A method for establishing the boundary condition along the free surface has been presented, along with the modeling of the pressure-strain term. The interaction of mean strain with fluctuating velocities ($\pi_{i,j,2} + \pi_{j,i,2}$) is finally modeled as shown in Table 1.

The wall effect term ($\pi_{i,j,w} + \pi_{j,i,w}$) on turbulent stresses is modeled as shown in Table 1 by changing the model constants. In Table 1, $f(L/X_w)$ is a function related to the dimensionless distance from the wall, and c_μ and κ represent the empirical constant and the von Karman constant, respectively. The function $f(L/X_w)$ is that of a unit value near the wall, which approaches zero with increasing distance from the wall. The symbol X_w is the normal distance from the wall, and L defines the length scale of turbulence. When $f(L/X_w)$ is zero, the model yields the correct Reynolds stress components for the nearly homogeneous shear flow of Champagne et al. (1970). In contrast, when $f(L/X_w)$ is of unit value, the magnitude of the stress components agrees with the consensus of the near wall turbulence. The model constants used in this analysis are summarized in Table 2.

The fourth term on the right-hand side of Equation (2) is the homogeneous part of dissipation. The dissipation rate everywhere in the computed flow was assumed to be locally isotropic, i.e.

Table 2 Model constants of the pressure-strain correlation term

C_1^*	C_2^*	ζ^*	C_1'	C_2'	ζ'	C_μ	κ
1.4	0.44	-0.16	-0.35	0.12	-0.1	0.09	0.42

$$\varepsilon_{ij} = 2\nu \frac{\partial u_i}{\partial X_k} \frac{\partial u_j}{\partial X_k} = \frac{2}{3} \delta_{ij} \varepsilon. \quad (8)$$

The transport equations of turbulent energy and dissipation are expressed in the following form:

$$\frac{Dk}{Dt} = \frac{\partial}{\partial X_j} \left\{ \left(\nu \delta_{jk} + c_s \frac{k}{\varepsilon} \overline{u_k u_j} \right) \frac{\partial \varepsilon}{\partial X_k} \right\} - \overline{u_i u_k} \frac{\partial U_i}{\partial X_k} - \varepsilon, \quad (9)$$

$$\frac{D\varepsilon}{Dt} = \frac{\partial}{\partial X_j} \left\{ \left(\nu \delta_{jk} + c_\varepsilon \frac{k}{\varepsilon} \overline{u_k u_j} \right) \frac{\partial \varepsilon}{\partial X_k} \right\} - \frac{\varepsilon}{k} \left(c_{1\varepsilon} \overline{u_i u_k} \frac{\partial U_i}{\partial X_k} - c_{2\varepsilon} \varepsilon \right). \quad (10)$$

Model constants c_s , c_ε , $c_{1\varepsilon}$ and $c_{2\varepsilon}$ are 0.22, 0.18, 1.44, and 1.92, respectively.

2.3 Wall Function

In the proposed turbulent model, the wall function method is used to set the boundary conditions for turbulent energy and dissipation. Adopting the wall function method along the walls, it is necessary to obtain the values of turbulent energy and dissipation in order to assume the log-law velocity profile over the walls. The following log-law velocity profile for a smooth wall is assumed for this study:

$$\frac{U}{U_\tau} = \frac{1}{0.42} \ln \left(\frac{U_\tau y}{\nu} \right) + 5.5. \quad (11)$$

2.4 Numerical Analysis

Figure 2 shows the cross-section of the computational grids. The computational sub-channels have a width of $0.876 D$ and height of $1.084 D$. They are connected by the gap with a width of $0.122 D$ and a height of $0.061 D$. Although these geometric lengths are the same as the experiment, they have a length of $75 D$, which is longer than the experiment, $42.1 D$. The computational measuring plane is also performed at $X_1 = 41.96 D$. The gap vorticity distribution is presented in the gap-center plane at $X_3 = 1.053 D$. These positions of the measuring planes are also the same as the experiment.

Three inlet values of the turbulent energy are assumed to be $k/U_b^2 = 1 \times 10^{-5}$, 1×10^{-2} and 6×10^{-2} . All the figures shown in this study except Fig. 10 are the results when $k/U_b^2 = 6 \times 10^{-2}$. The initial value of turbulent dissipation is assumed to be $\varepsilon = k^{3/2}/D$. The wall function is adopted as the boundary condition for the turbulent energy and dissipation at the first grid point from the wall. Fine grids are used near the

wall because the physical parameters change rapidly near the wall. The governing equations are discretized by the differencing scheme and QUICK (a third-order up-wind differencing scheme) is used for the convection term. The computational Reynolds number is 2×10^5 , based on the hydraulic diameter and the bulk velocity. The total cross-section has 85×43 computational grid points, and 250 grid points are set along the axial flow direction. Therefore, the total number of computational grids is 913 750.

3. RESULTS

The calculated results for the mean axial flow velocities are compared with the data of the experiment at $X_1/D = 41.96$ as shown in Figure 3. The velocity is dimensionless by the bulk velocity of the channel. In all four corners, the isocontours of the axial velocity are bulged. In the experiment, the isocontours were obviously stretched to the gap and there was a large difference between the flow near the corner with the gap and that near the other three corners. The experimental result showed how the effect of the large scale pulsation was large on the velocity distribution. However, the calculated isocontours are stretched slightly, not as much as those of the experiment.

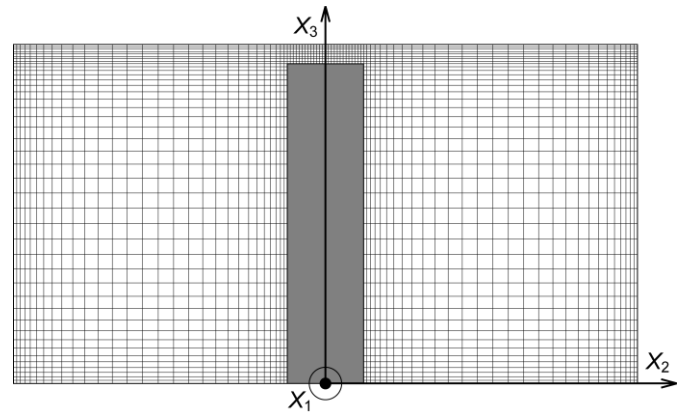


Fig. 2 Cross-section of the computational grids

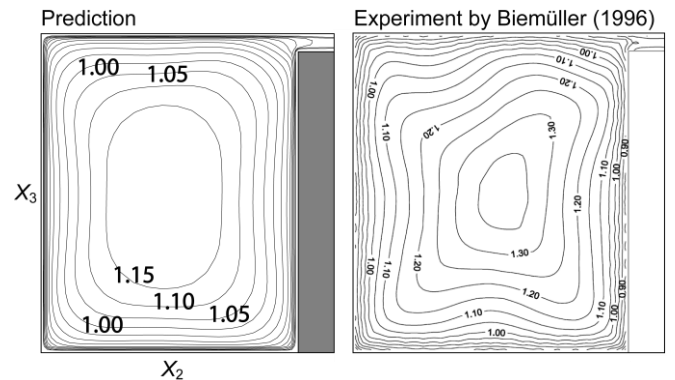


Fig. 3 Mean axial flow velocity contours

The calculated isocontours of the axial (X_1 -direction) turbulence intensity divided by the average friction velocity are compared with the result of the experiment in Fig. 4. The contours are in good agreement with the experiment qualitatively and quantitatively. The minimum value of the intensity is predicted less than 0.80 and the maximum is predicted about 1.9 near the gap. The predicted values of the axial turbulence intensity are less than the experiment in the entire plane.

The calculated isocontours of the turbulence intensity in the horizontal direction (X_2 -direction) are compared with the result of the experiment in Fig. 5. The data are also made dimensionless by the average friction velocity. The location of the lowest value was measured in the center of the channel in the experiment. While, the calculated location of the lowest value is predicted on the left. The predicted maximum peak at the beginning of the gap is about 1.5 near the top wall, but that is less than that in the experiment. However, the minimum is about 0.8 what is also detected in the experiment.

Figure 6 shows the isocontours of the dimensionless turbulent shear stress by the square of the average friction velocity. In the lower half of the channel, the result is in good agreement with the experiment and also with the result obtained in the experiment for the square duct with no gaps by Melling (1976). As shown in the experiment, zero-line is slightly transversed to the left in the upper half. The very high peak observed in the experiment is not predicted at the beginning of the gap. The maximum value at the point is about 0.4 and is much lower than that in the experiment. In a major part of the channel, the shear stress decreases from left to right. That is usual as the distribution for rectangular channels.

The calculated instantaneous vorticity distribution in the gap-center horizontal plane is presented in Fig. 7 in which the gap is indicated in gray on the left. The rotation axis of the vorticity is parallel to the X_3 axis. The clockwise vorticity is painted in blue and the counter-clockwise in red. The positive and negative shear layers start to wave where $15 < X_1/D < 20$. Positive vorticity regions are predicted periodically on the concave of the waving negative shear layers as well as negative ones. The centers of the vortices are outside of the gap, although large eddy simulation by Biemüller predicted that the centers were within the gap.

Figure 8 shows the longitudinal vorticity distribution in the plane at $X_1/D = 41.96$. The rotation axis of the vorticity is parallel to the stream direction and the counter-clockwise vorticity is painted in red. In the three corners without the gap, pairs of vortices induced by the secondary flow of the second kind are predicted. Although the pair of the vortices in the corner with the gap is also observed, the positive vorticity region is larger than the negative one. The positive is induced obviously by the flow from the gap, i.e. the large scale pulsation.

At the gap center $(X_2/D, X_3/D) = (0, 1.053)$, the horizontal velocity U_2 changes periodically and the change is convected toward downstream as shown in Fig. 9. The horizontal axis of the figure is X_1/D and the vertical axis is the dimensionless time, $t U_b/D$. The velocity is painted in red when the direction is from the left sub-channel to the right one and the

magnitude is more than 10% of the bulk velocity. The velocity starts to fluctuate periodically in the $X_1/D > 20$ region.

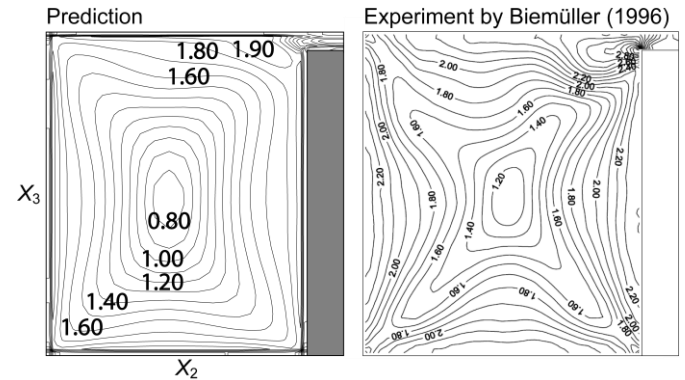


Fig. 4 Isocontours of the turbulence intensity in the axial direction ($\sqrt{u_1^2}/U_\tau$)

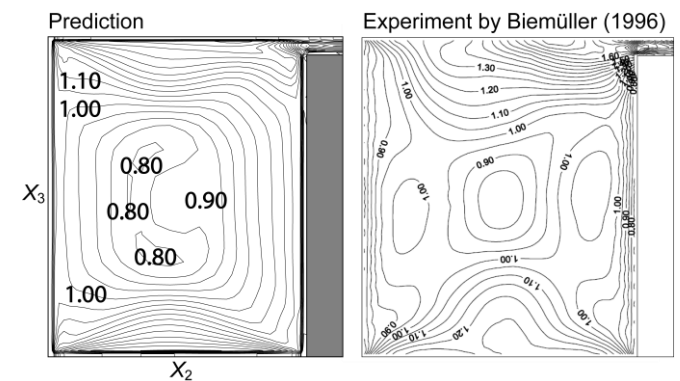


Fig. 5 Isocontours of the turbulence intensity in the horizontal direction ($\sqrt{u_2^2}/U_\tau$)

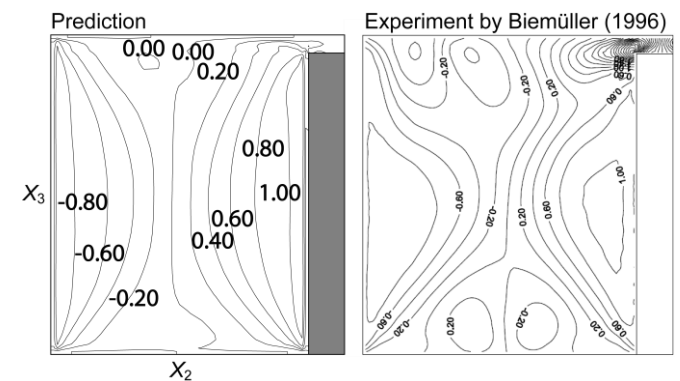


Fig. 6 Isocontours of the turbulent shear stress ($\overline{u_1 u_2}/U_\tau^2$)

Figure 10 shows the rms value of the dimensionless horizontal velocity, U_{2rms}/U_b , and the dimensionless axial mean velocity, U_{1mean}/U_b , at the gap-center for three inlet conditions of the turbulent energy versus X_1/D . U_2 is able to be interpreted into the inter-channel mixing rate per unit area. Therefore the rms value, U_{2rms}/U_b , is the amplitude of the inter-channel mixing rate. When $k/U_b^2 = 6.0 \times 10^{-2}$, the mean velocity has the minimum value of 0.275 at $X_1/D = 17.2$. From the inlet to this location, the pairs of the longitudinal vortices induced by the secondary flow of the second kind seem to become larger. However, in the corner with the gap, the secondary flow can not turn at the corner but get into the gap. Therefore, the pair of the vortices also gets in the gap. In addition, the fluctuation has a small value of 0.00778 at the location. These indicate that the secondary flows with larger

momentum from the left and the right channels get into the gap and they are ballanced. From this location, the fluctuation is increased to 0.0727 and the mean velocity is also increased to 0.589. The secondary flows seem to make the mean axial velocity increased and to lose the balance. It is suggested that the secondary flow of the second kind induces the large scale pulsation. When $k/U_b^2 = 1.0 \times 10^{-5}$, the mean velocity has the minimum value of 0.269 at $X_1/D = 14.5$. From this location the fluctuation is increased from 0.0127 to 0.0709 and the mean velocity is also increased to 0.586. It is suggested that the large trubulent energy is able to make the beginning of the large scale pulsation downstream.

4. CONCLUSIONS

A numerical analysis has been performed using an

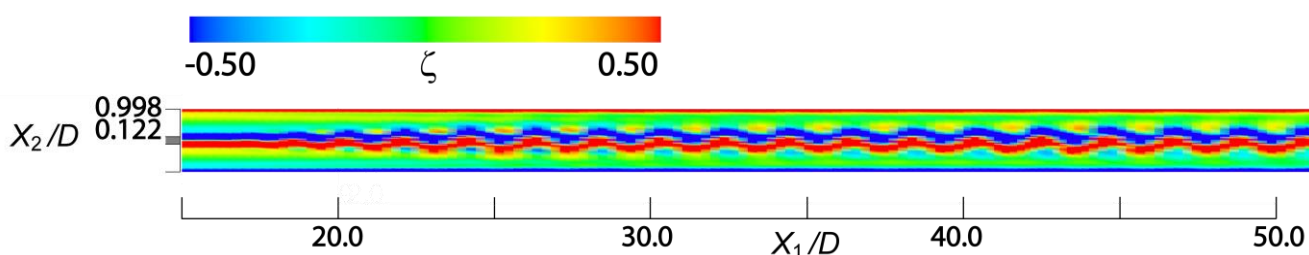


Fig. 7 Calculated instantaneous vorticity distribution in the gap-center horizontal plane

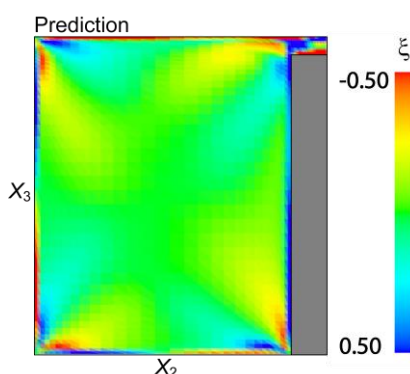


Fig. 8 Longitudinal vorticity distribution in the plane where $X_1/D = 41.96$

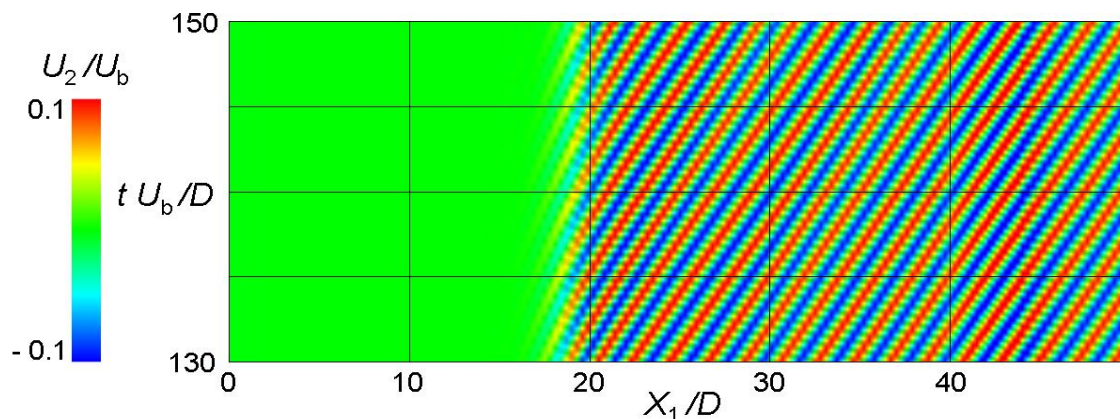


Fig. 9 Calculated horizontal velocity in the gap center vs. dimensionless time

algebraic Reynolds stress model for a three-dimensional turbulent flow in the two rectangular channels connected by a gap. This turbulent flow is characterized by the inter-channel flow through the gap, i.e. the large scale pulsation. The calculated results are compared quantitatively with the result of the experiment measured by Biemüller to confirm the validity of the proposed method. The following conclusions are obtained based on the numerical analysis:

1. The present method can predict the isocontours of the mean velocity, the axial turbulence intensity and the turbulent shear stress qualitatively and quantitatively.
2. The predicted isocontours of the turbulence intensity in the horizontal direction indicates a slight difference from the experimental results qualitatively.
3. The calculated vorticity distributions show the periodic large scale pulsation and the unbalanced pair of the longitudinal vortices.
4. In the center of the gap, the mean axial velocity and the rms value of the horizontal velocity are increased at the same location and it is suggested that the location depends upon the inlet turbulent energy.
5. Algebraic Reynolds stress model is able to predict the experimental feature qualitatively and quantitatively.

ACKNOWLEDGEMENTS

The results of this study are performed on the re-entrainment from the LWR hydrogen safety program of the Japan Atomic Energy Agency, which is funded by the Ministry of Economy, Trade and Industry.

REFERENCES

- Biemüller, M. et al., 1995, Eng. Turb. Model. Exp., Vol. 3, pp 249-253.
- Champagne, F.H. et al., 1970, J. Fluid Mech., Vol. 41, pp. 81-139.
- Gessner, F.B. et al., 1981, Procs. 3rd Symp. Turb. Shear Flows, pp. 25-32.
- Guellouz, M. S. et al., 2000, Exp. Therm. Fluid Sci., Vol. 23, pp 59-73.
- Launder, B.E. et al., 1975, J. Fluid Mech., Vol. 22, pp. 537-566.
- Melling, A. et al., 1976, J. Fluid Mech., Vol. 78, pp. 289-315.
- Meyer, L., 2010, Nucl. Eng. Design, Vol. 240, pp. 1575-1588.
- Rodi, W., 1976, Zeitschrift für Angewandte Mathematik und Mechanik, Vol. 56, pp. 219-221.
- Sugiyama, H. et al., 2005, Intl. J. Num. Methods in Fluids, Vol. 47, pp. 1431-1449.
- Sugiyama, H. et al., 2006, Intl. J. Num. Methods in Fluids, Vol. 51, pp. 791-818.
- Sugiyama, H. et al, 2014, Proc. JSAE automn conf., pp. 5-11.

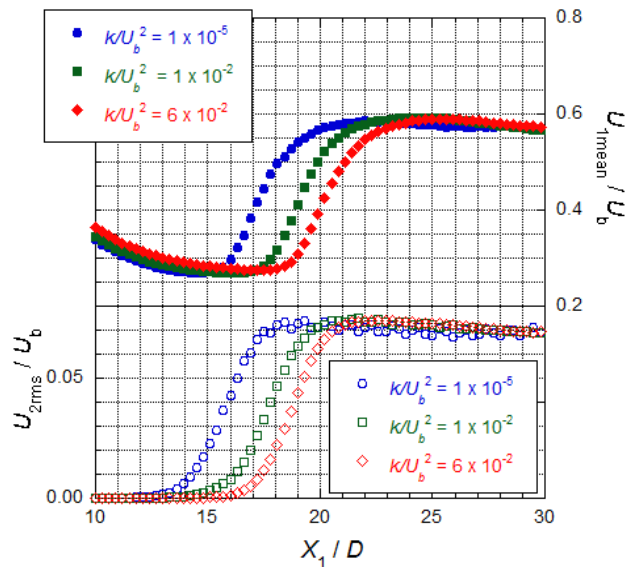


Fig. 10 Axial mean velocity and horizontal velocity fluctuation versus X_1/D